

DLFR-VAE: Dynamic Latent Frame Rate VAE for Video Generation

Zhihang Yuan^{*1,2} Siyuan Wang^{*1} Rui Xie^{1,2} Hanling Zhang^{1,2} Tongcheng Fang^{1,2} Yuzhang Shang³
Shengen Yan² Guohao Dai^{4,2} Yu Wang¹

Abstract

In this paper, we propose the Dynamic Latent Frame Rate VAE (**DLFR-VAE**), a training-free paradigm that can make use of adaptive temporal compression in latent space. While existing video generative models apply fixed compression rates via pretrained VAE, we observe that real-world video content exhibits substantial temporal non-uniformity, with high-motion segments containing more information than static scenes. Based on this insight, DLFR-VAE dynamically adjusts the latent frame rate according to the content complexity. Specifically, DLFR-VAE comprises two core innovations: ❶ a Dynamic Latent Frame Rate Scheduler that partitions videos into temporal chunks and adaptively determines optimal frame rates based on information-theoretic content complexity, and ❷ a training-free adaptation mechanism that transform pretrained VAE architectures to dynamic VAE that can process features with variable frame rates. Our simple but effective DLFR-VAE can function as a plug-and-play module, seamlessly integrating with existing video generation models and accelerating the video generation process.

1. Introduction

Video is a fundamental medium for capturing real-world dynamics, making the generation of diverse video content a crucial capability for AI systems [Brooks et al., 2024; Agarwal et al., 2025]. Recent advances in diffusion models [Ho et al., 2020; Rombach et al., 2022; Esser et al., 2024; Jin et al., 2024] and autoregressive models [Kuaishou, 2024; Fan et al., 2024] have led to notable breakthroughs in producing high-fidelity and long-duration videos.

At the heart of these video generation frameworks lies the Variational Autoencoder (VAE) [Kingma, 2013; Rombach et al., 2022; Xing et al., 2024], which jointly reduces spatial and temporal dimensions to create compact latent rep-

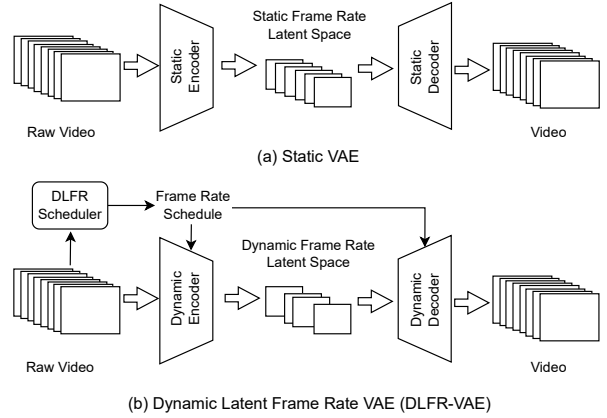


Figure 1. **DLFR-VAE**: A training-free approach that accelerates video generation through content-adaptive spatial-temporal compression. This module can seamlessly integrate with existing pretrained video generative models.

resentations. This latent space not only provides a more structured manifold for downstream generative tasks, but also substantially lowers computational and memory requirements compared to operating in the original video domain [Agarwal et al., 2025; Brooks et al., 2024]. Based on the latent space, modern architectures, such as Diffusion Transformers [Peebles & Xie, 2023] or Auto-Regressive Transformers [Esser et al., 2021], can then effectively learn the distribution of these latent representations, with the VAE decoder ultimately reconstructing them back into complete videos [Jin et al., 2024; Kuaishou, 2024; Kong et al., 2024].

The computational complexity of video generation is largely determined by the size of the latent representation (*i.e.*, the number of latent tokens) [Kong et al., 2024; Zheng et al., 2024; Kondratyuk et al., 2023]. This substantial token count imposes significant computational overhead, primarily due to the quadratic complexity of attention in diffusion and autoregressive Transformers [Vaswani, 2017; Kondratyuk et al., 2023; Peebles & Xie, 2023]. Therefore, addressing this bottleneck is pivotal for extending video generation to longer durations and higher resolutions.

In order to achieve more efficient video generation in a training-free manner, we explore the possibility of adjusting latent frame rates based on information-theoretic content density. Prior studies have demonstrated that video data exhibits significant temporal non-uniformity [Feichtenhofer

^{*}Equal contribution. ¹Tsinghua University ²Infinigence AI ³Illinois Tech ⁴Shanghai Jiao Tong University.

et al., 2019; Yang et al., 2020; Li et al., 2022]. For example, high-motion segments (e.g., soccer shots) have more content complexity than static scenes (e.g., stationary players). Our empirical observations reveal that in standard fixed-rate latent spaces, roughly 35% of latent units carry minimal information, indicating considerable computational waste. These findings support our key motivation: sparse-content segments (e.g., slow-motion sequences) can be efficiently represented with fewer latent elements, whereas dense-content segments require a higher token density to preserve temporal complexity [Yu et al., 2024; Xiang et al., 2020; Lin et al., 2023; Ravanbakhsh et al., 2024].

Based on this motivation, we propose **Dynamic Latent Frame Rate VAE, DLFR-VAE**, a novel framework that enables dynamic frame rate in the latent space without additional training. We propose two key technical innovations for DLFR-VAE: ❶ a Dynamic Latent Frame Rate Scheduler that partitions videos into temporal chunks and adaptively determines optimal frame rates based on content complexity, and ❷ a training-free adaptation mechanism that enables pretrained VAE architectures to process features with variable frame rates. This dynamic frame rate strategy can significantly reduce both computational overhead and memory requirements for video generative models (See Fig. 1).

The first component ❶ centers on our efficient content complexity metric based on inter-frame differences, which enables real-time frame rate adaptation during inference with minimal computational overhead. We can then schedule each video chunk’s adaptive frame rate based on this metric. Building on this scheduler, we develop ❷ a training-free mechanism to augment pretrained VAE models with dynamic frame rate capabilities. Leveraging the robust compression and reconstruction capabilities of large-scale pretrained video VAEs [Wu et al., 2024b; Xing et al., 2024; Chen et al., 2024], we strategically inject dynamic sampling modules into the network architecture. In the encoder, we incorporate dynamic downsampling operators that modulates frame rates, producing chunk features with varying temporal resolutions. The decoder mirrors this design with dynamic upsampling operators that restores features to a consistent frame rate. This architectural approach preserves pretrained weights while enabling dynamic frame rate control, making DLFR-VAE a plug-and-play module for downstream video generative models.

Experimental results show that DLFR maintains a reconstruction quality (SSIM change < 0.03) while reducing the average number of latent space elements by 50%. We integrated DLFR into an existing diffusion-based video generation model without any fine-tuning, and the model was able to generate acceptable videos with a significant speedup. The latency of a diffusion step is reduced by 2 to 6 times, and the end to end speedup is 2x to generate a video.

2. Related Work

2.1. Autoencoders for Visual Generation Models

Visual generation in high-resolution pixel space imposes prohibitive computational costs for diffusion and autoregressive models. To address this, Rombach et al. [2022] introduced latent diffusion models operating in compressed spaces via pretrained autoencoders [Kingma, 2013]. The standard design employs an $8\times$ spatial compression ratio with four latent channels [Peebles & Xie, 2023; Li et al., 2024b; Tian et al., 2024]. Recent works have focused on improving reconstruction quality through increased latent channels [Esser et al., 2024] or enhanced decoders with task-specific priors [Zhu et al., 2023].

In contrast, our work targets a different but equally important goal: dynamically increasing the spatial compression ratio of autoencoders while still maintaining acceptable reconstruction quality. Chen et al. [2024] also address high compression ratios to enable efficient high-resolution diffusion models; however, their approach trains a specialized autoencoder. Our method, by comparison, is training-free, allowing us to obtain a more compressed latent space without retraining the original autoencoder. To our knowledge, this is the first study to explore higher compression ratios in this training-free manner.

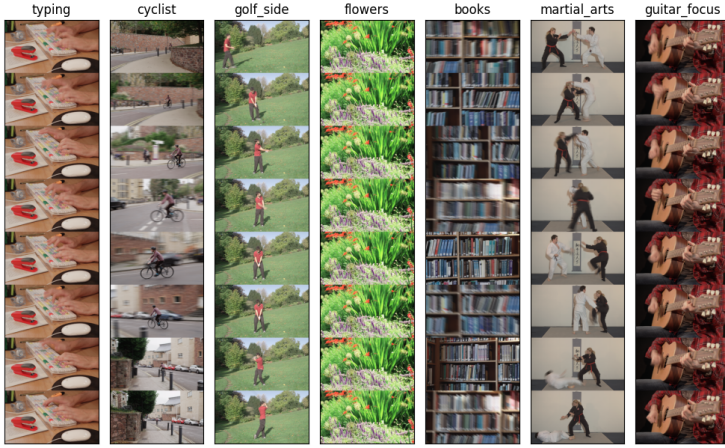
2.2. Training-free Acceleration for Generative Models

The computational intensity of generative models has spurred various acceleration strategies, with training-free methods gaining prominence due to the high training costs of modern architectures [Ma et al., 2024b]. Key approaches include: (1) Reducing inference sampling steps through training-free few-step samplers [Song et al., 2020; Lu et al., 2022a;b; Zhang & Chen, 2022]; (2) Model compression via sparsity [Ma et al., 2024a; Yuan et al., 2024] or quantization [Shang et al., 2023; Li et al., 2023; Wang et al., 2024; Wu et al., 2024a; Li et al., 2024a].

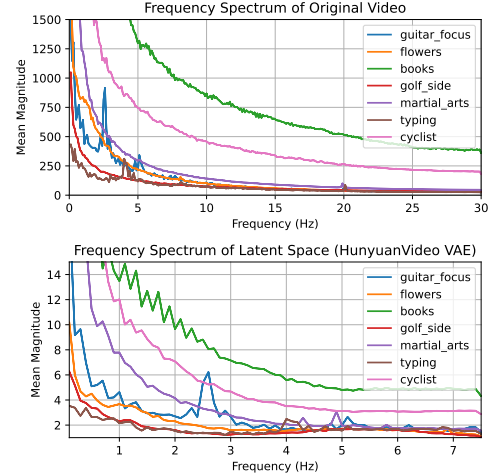
While these methods focus on optimizing diffusion or autoregressive backbones, they leave the autoencoder unchanged. Our approach introduces a novel direction: enhancing video generation efficiency by increasing video autoencoder compression ratios without additional training, thereby reducing overall computational demands.

3. Method

In this section, we present DLFR-VAE, a training-free solution for dynamic frame rate control in the latent space. We first establish our theoretical foundation by analyzing the temporal frequency of video signals in both pixel and latent spaces (Sec. 3.1). Based on this analysis, we propose our dynamic latent frame rate space (Sec. 3.2). To realize



(a) Example video segments in BVI-HFR [Mackin et al., 2018]. Each one is 10 seconds at 1080p/60Hz. The “cyclist” and “books” demonstrates rapid camera motion, while “flowers” and “typing” contain slower, more static content.



(b) Temporal frequency analysis comparing original video signals (top) and their latent space representations from HunyuanVideo VAE (bottom) [Kong et al., 2024].

Figure 2. Analysis of temporal frequency characteristics in both pixel and latent spaces. Key observations: (1) Fast-motion segments exhibit higher temporal frequency content in both domains, while static scenes show concentrated low frequency. (2) The latent space preserves the relative frequency patterns of the original signals, enabling content-adaptive frame rate compression in the latent domain.

this design, we propose two key technical components: ❶ a Dynamic Latent Frame Rate Scheduler that determines optimal frame rates based on content complexity (Sec.3.3), and ❷ a training-free adaptation mechanism that enables pretrained VAE architectures to process variable frame rate features (Sec.3.4). Beyond these components, we provide a more straightforward explanation for why our simple yet effective approach can work (Sec.3.5).

3.1. Motivation

Traditional frame rate optimization in video processing and compression has predominantly focused on raw video signals [Song & Kuo, 2001; Mackin et al., 2015]. Previous studies in video content analysis have demonstrated that video information density exhibits strong temporal non-uniformity. This non-uniformity manifests as significant variations in temporal frequency across different video segments [Menon et al., 2022; Papakonstantinou, 2023]. For instance, in our analysis of the BVI-HFR dataset (Fig. 2a), fast-motion sequences like “books” exhibit 5–8× higher temporal frequency magnitude compared to static scenes like “flowers” (see Fig.2b Top).

However, with the growing adoption of deep learning for video generation, videos are increasingly mapped into a latent space via an encoder [Fan et al., 2024; Kuaishou, 2024; Zheng et al., 2024; Kong et al., 2024]. This raises crucial questions: (i) *How do temporal characteristics transfer into the latent space?* (ii) *Does the latent space preserve the frequency variations observed in the original pixel domain?* (iii) *Can we apply dynamic frame rates within the latent space?* Although these questions are highly relevant, all of them remain underexplored.

Frequency Analysis of Signals. A continuous-time signal can be denoted as $x(t)$. Its frequency spectrum $X(f)$ is obtained via the Fourier transform, and for a band-limited signal, it is nonzero only up to a maximum frequency f_{\max} :

$$X(f) = 0, \quad \forall |f| > f_{\max}. \quad (1)$$

Sampling the continuous signal at sampling frequency F_s discretizes $x(t)$ into frames:

$$x[n] = x(nT), \quad T = \frac{1}{F_s}. \quad (2)$$

According to the Nyquist-Shannon sampling theorem [Nyquist, 1928; Shannon, 1949], F_s must satisfy

$$F_s \geq 2f_{\max}. \quad (3)$$

to prevent aliasing. As f_{\max} varies across different segments of the signal, different segments naturally require different frame rates, motivating adaptive frame rate strategies.

Temporal Frequency Analysis of Latent Space. Let the video luminance signal be $x(t)$, and its encoder mapping be \mathcal{E} . In the latent space, the signal becomes $z(t) = \mathcal{E}(x(t))$ with a corresponding frequency spectrum $Z(f)$:

$$Z(f) = \int_{-\infty}^{\infty} z(t)e^{-j2\pi ft} dt. \quad (4)$$

Note that \mathcal{E} is a complex nonlinear transformation, it can alter the amplitude, phase, and frequency characteristics of a signal or generate new frequency components, leading to changes in the video signal’s shape and spectrum. Therefore, we first analyze the signal in the latent space.

Through empirical analysis on multiple video segments (see Fig. 2b), we observe pronounced frequency variability in both the original video domain and latent domain. High-speed segments—such as rapid camera pans or fast-moving objects—often retain higher temporal frequencies, whereas low-motion segments focus on lower-frequency components. This suggests that adaptive frame rate optimization remains viable in latent space, just as it is in raw pixel space.

In line with the Nyquist-Shannon theorem, when the latent-space sampling rate F'_s meet

$$F'_s \geq 2f'_{\max}, \quad (5)$$

aliasing can be prevented. The f'_{\max} is its maximum frequency in latent space. Hence, segment-wisely estimating f'_{\max} and adjusting F'_s provides an opportunity to implement a variable frame rate in latent space.

3.2. Dynamic Frame Rate Latent Space

Building on the above analysis, we propose a dynamic frame rate latent space wherein each video segment can have a distinct frame rate, allocated based on its temporal complexity. Specifically, suppose an input video is divided into M segments $\{S_1, \dots, S_M\}$, each comprising N frames. For segment S_i , its latent representation is $z_i(t)$. The frequency spectrum $Z_i(f)$ is defined as

$$Z_i(f) = \int_{t_i}^{t_i+NT} z_i(t) e^{-j2\pi ft} dt, \quad (6)$$

where $T = 1/F_s$ is the sampling interval in the raw video domain.

From empirical observations, certain high-frequency components in $Z_i(f)$ have negligible amplitude and minimal impact on overall fidelity. We thus define an effective maximum frequency $f_{\text{eff},i}$ for each segment, identifying the point where the amplitude remains above a threshold ϵ :

$$f_{\text{eff},i} = \max\{f \mid |Z_i(f)| \geq \epsilon\}. \quad (7)$$

By the Nyquist-Shannon principle [Ash, 2012], the corresponding latent-space frame rate for segment S_i can be lowered to

$$F'_{s,i} = 2f_{\text{eff},i}. \quad (8)$$

This adaptive sampling ensures each segment maintains only the minimum frame rate necessary to preserve perceptually significant temporal details. To maintain temporal consistency across segment boundaries, we implement a smooth transition mechanism that gradually adjusts frame rates between adjacent segments.

3.3. DLFR Scheduler

While theoretically sound, computing exact frequency spectra for real-time video processing presents significant com-

putational challenges. We address this through a practical approximation strategy that maintains the benefits of dynamic frame rates while ensuring computational efficiency. Our approach discretizes the continuous space of temporal complexities into N distinct levels. Each level $k \in \{1, \dots, N\}$ is associated with an effective frequency $f'_{\text{eff},k}$ ¹. If segment S_i falls into complexity class k , its latent frame rate becomes

$$F'_{s,i} = 2f'_{\text{eff},k}. \quad (9)$$

Formally, we express this as:

$$F'_{s,i} = \sum_{k=1}^N (2f'_{\text{eff},k}) \mathbb{I}_{C_k}(S_i), \quad (10)$$

where $\mathbb{I}_{C_k}(S_i)$ is an indicator function that is 1 if S_i belongs to class C_k and 0 otherwise.

Directly evaluating $\mathbb{I}_{C_k}(S_i)$ from raw or latent signals can still be challenging. Instead, we use a practical content complexity metric $C(S_i)$ as a proxy, which considers the SSIM of adjacent frames in a raw video segment:

$$C(S_i) = \frac{1}{N} \sum_{j=1}^{N-1} (1 - \text{SSIM}(x[j], x[j+1])), \quad (11)$$

This metric can efficiently distinguish high-motion segments from low-motion ones without explicitly analyzing the latent frequency spectrum. The scheduling logic then maps each segment’s metric value to an appropriate complexity class k , and hence to a frame rate $F'_{s,i}$. As illustrated in Figure 4, the content complexity metric exhibits a high correlation with both the effective frequency and the VAE reconstruction performance. We use this metric and thresholds Th to determine the frame rate:

$$\mathbb{I}_{C_k}(S_i) = \begin{cases} 1, & \text{if } Th_i^{\text{down}} < C(S_i) \leq Th_i^{\text{up}} \\ 0, & \text{else.} \end{cases} \quad (12)$$

3.4. Transform Static VAE to Dynamic VAE

To convert a pretrained static-frame VAE into a dynamic-frame version, we exploit the existing capacity of modern video VAEs, which have learned to compress videos into fixed-frame latent spaces [Chen et al., 2024; Xing et al., 2024; Zhu et al., 2023]. As illustrated in Fig. 3, our approach introduces two key modifications to the pretrained VAE: a dynamic downsampling module in the VAE’s encoder and a corresponding upsampling module in the decoder. This design allows us to leverage the robust compression capabilities of pretrained VAEs while enabling variable frame rate processing without requiring additional training.

¹For example, we use $\{1, 2, 4\}$ Hz for the 16 FPS video, which have $\{16x, 8x, 4x\}$ temporal downsample ratio.

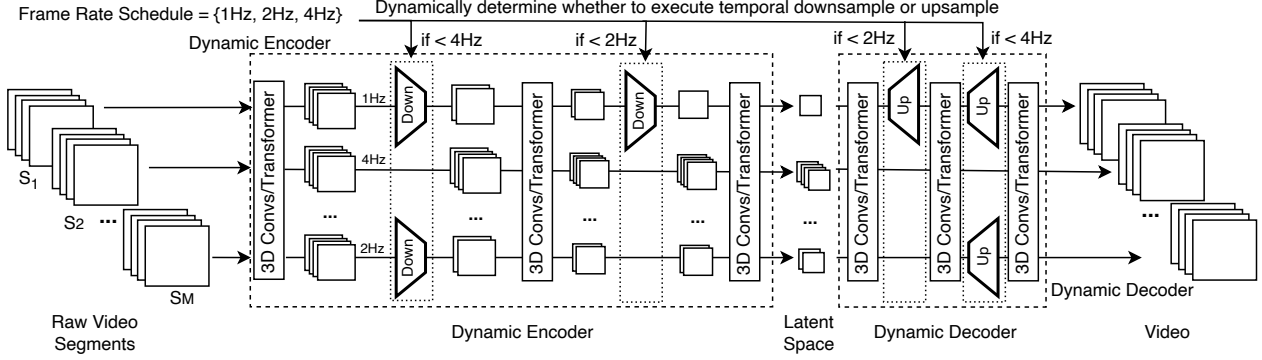


Figure 3. **Architecture overview of the Dynamic Latent Frame Rate (DLFR) VAE.** The input video is first divided into segments. The dynamic encoder processes these segments through a series of 3D convolution layers interspersed with dynamic downsample operations (Eq. 13 in Sec. 3.4), where the execution of downsample is determined by the schedule (Sec. 3.3). The resulting latent representations maintain varying temporal resolutions according to segment complexity (Sec. 3.2). The dynamic decoder then reconstructs the video through corresponding upsampling operations (Eq. 15 in Sec. 3.4), restoring the original frame rate while preserving temporal consistency. Each segment can be processed at different frame rates, enabling content-adaptive temporal compression in latent space.

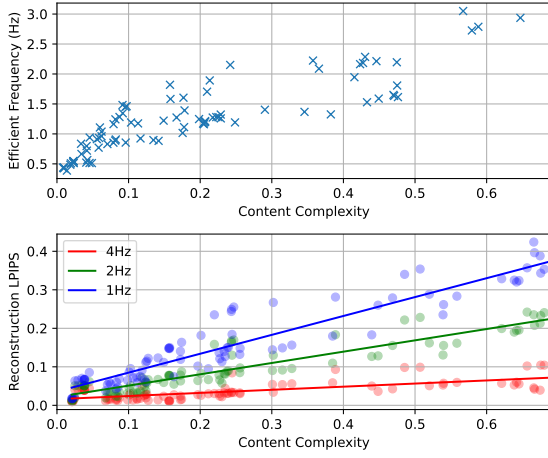


Figure 4. **Content complexity experiment on HunyuanVideo VAE.** The upper figure illustrates the relationship between content complexity and effective frequency, with $\epsilon = 1.8$ used in this experiment. The lower figure demonstrates the alignment between content complexity and reconstruction LPIPS, indicating a strong correlation.

Encoder Modification. Let the input video be $\{x_1, x_2, \dots, x_T\}$. A pretrained video VAE encoder E typically processes this input into a latent representation z . To support variable frame rates, we introduce a dynamic downsampler at a strategically chosen point in the encoder. Given a frame-rate schedule $\{F'_{s,1}, F'_{s,2}, \dots, F'_{s,M}\}$, the downsampler transforms encoder features h_i for each segment S_i into a reduced-rate feature h'_i :

$$h'_i = \text{Downsample}(h_i, F'_{s,i}). \quad (13)$$

These reduced-rate features are then passed through the remaining encoder layers, denoted E_{post} , to yield segment-

wise latent codes $\{z_1, \dots, z_M\}$.

Decoder Modification. Decoding requires reversing the frame rate changes. A dynamic upsampler is inserted at the corresponding decoder stage. For each segment’s latent code z_i , the initial decoder layers D_{pre} produce intermediate features h''_i :

$$h''_i = D_{\text{pre}}(z_i). \quad (14)$$

The upsampler then restores the original frame rate F_s :

$$h'''_i = \text{Upsample}(h''_i, F_s), \quad (15)$$

after which the remaining decoder layers D_{post} reconstruct the final segment \hat{S}_i . The overall video reconstruction \hat{V} is formed by concatenating $\{\hat{S}_1, \dots, \hat{S}_M\}$.

Crucially, these modifications allow the pretrained encoder and decoder weights to remain largely unchanged, except for the newly inserted downsampling and upsampling operators. Consequently, DLFR-VAE can be deployed as a training-free extension on top of mainstream video VAEs, seamlessly enabling dynamic latent frame rate control.

3.5. Discussion on DLFR-VAE

In addition to our information-theoretic formulation, we offer an intuitive explanation for why our **simple but effective** DLFR-VAE can compress latent space with minimal reconstruction loss. At its core, DLFR-VAE dynamically downsamples the pretrained VAE encoder and, in turn, upsamples its decoder—effectively achieving content-dependent spatial-temporal compression without additional training as shown in Fig. 3.

Pretrained video VAEs [Chen et al., 2024; Xing et al., 2024; Zhu et al., 2023] are typically trained on large-scale datasets

that include diverse motion types, ranging from slow to fast, and from sparse to dense. Many training pipelines also involve augmentation techniques (e.g., temporal interpolation) that effectively expose the VAE to slower versions of the same content. Consequently, the VAE develops an internal capacity to represent video content at different temporal scales, but its default latent space is merely configured to operate at a fixed frame rate. DLFR-VAE can thus be seen as a mechanism that “reactivates” this dormant flexibility. By strategically downsampling and upsampling in the encoder and decoder, respectively, *we allow the VAE to adapt to each segment’s temporal complexity, leveraging the latent representational power that was already learned but not previously utilized for frame rate variation.*

4. Experiment

To evaluate the performance of the proposed DLFR-VAE framework, we applied it to two state-of-the-art pretrained VAE models: *HunyuanVideo VAE* [Kong et al., 2024] and *Open-Sora 1.2 VAE* [Zheng et al., 2024]. These models were converted into Dynamic VAEs by incorporating our dynamic frame rate mechanism. We then tested their video reconstruction performance on a diverse set of videos.

4.1. Video Reconstruction

We conducted extensive experiments to compare the reconstruction quality of videos processed by the original VAE, Static VAE, and Dynamic VAE under different temporal compression ratios (CR). For evaluation, we used three commonly employed metrics: SSIM, PSNR, and LPIPS [Zhang et al., 2018]. Lower LPIPS values indicate better perceptual quality, while higher SSIM and PSNR values signify better structural and pixel-level fidelity.

To test the effects of dynamic characteristics in videos, we used the **BVI-HFR dataset** [Mackin et al., 2018], which includes a variety of scene types and motion patterns, such as dynamic textures and fast-moving objects against static backgrounds. We evaluated videos at two resolutions (**540p** and **720p**) and two frame rates (**15fps** and **30fps**).

For the original VAE, the temporal compression ratio is 4x. To convert the Static VAE into a Dynamic VAE, we modified the encoder and decoder by introducing Dynamic Downsampling and Dynamic Upsampling operators. For HunyuanVideo VAE, the encoder’s first two temporal strided convolution layers were augmented with a Dynamic Downsampling operator, while the decoder’s last two temporal strided convolution layers were enhanced with a Dynamic Upsampling operator. For Open-Sora VAE, we add the dynamic downsampling operators after the 2D VAE encoder, and the dynamic upsampling operators before the 2D VAE decoder. Both are a bilinear sample.

Table 1. Video reconstruction performance on HunyuanVideo VAE. CR indicates the temporal compression ratio. FVMD[Liu et al., 2024] (Frame-wise Video Motion Deviation) is specifically designed to capture the temporal coherence of inter-frame motion. Compared to the traditional rFVD metric, FVMD is more sensitive to unnatural motion transitions and provides a more accurate assessment of video smoothness and temporal consistency, aligning more closely with human perceptual judgments.

Size/FPS	VAE	CR	SSIM↑	PSNR↑	LPIPS↓	rFVD↓	FVMD↓
240p/15	Original	4x	0.698	23.82	0.08	116	623
240p/15	Static	8x	0.582	22.21	0.12	268	16514
240p/15	Static	16x	0.487	20.71	0.17	1244	17855
240p/15	Dynamic	6x	0.696	23.8	0.08	134	687
240p/15	Dynamic	8x	0.684	23.64	0.09	278	812
240p/15	Dynamic	12x	0.631	22.77	0.12	620	2345
240p/30	Original	4x	0.66	22.7	0.09	108	494
240p/30	Static	8x	0.59	21.7	0.11	196	13192
240p/30	Static	16x	0.5	20.6	0.15	1099	14777
240p/30	Dynamic	6x	0.661	22.7	0.09	127	508
240p/30	Dynamic	8x	0.655	22.6	0.09	324	815
240p/30	Dynamic	12x	0.62	22	0.11	571	1907
540p/15	Original	4x	0.806	27.27	0.071	57	331
540p/15	Static	8x	0.668	24.27	0.128	218	15134
540p/15	Static	16x	0.535	21.83	0.187	1281	16135
540p/15	Dynamic	6x	0.8	27.18	0.074	124	392
540p/15	Dynamic	8x	0.779	26.74	0.082	170	614
540p/15	Dynamic	12x	0.695	24.51	0.119	410	1766
540p/30	Original	4x	0.789	26.29	0.075	60	272
540p/30	Static	8x	0.682	24.05	0.118	155	11784
540p/30	Static	16x	0.562	21.84	0.172	1083	13222
540p/30	Dynamic	6x	0.786	26.23	0.076	131	300
540p/30	Dynamic	8x	0.773	26	0.082	156	526
540p/30	Dynamic	12x	0.712	24.2	0.109	485	1825
720p/15	Original	4x	0.971	38.95	0.041	8	201
720p/15	Static	8x	0.806	30.71	0.109	163	15180
720p/15	Static	16x	0.65	25.32	0.173	1257	16345
720p/15	Dynamic	6x	0.962	37.97	0.045	34	291
720p/15	Dynamic	8x	0.927	35.47	0.057	132	463
720p/15	Dynamic	12x	0.834	30.95	0.095	304	1687
720p/30	Original	4x	0.97	38.95	0.041	8	200
720p/30	Static	8x	0.832	30.07	0.097	189	15180
720p/30	Static	16x	0.684	25.68	0.162	1257	16348
720p/30	Dynamic	6x	0.964	38.07	0.04	94	291
720p/30	Dynamic	8x	0.944	36	0.049	156	411
720p/30	Dynamic	12x	0.867	31.32	0.081	505	1687

The results in Tables 1 and 2 highlight the following key findings: 1. **Static VAE significantly reduces reconstruction quality:** Compared to the original VAE, inserting static downsampling and upsampling operators at higher compression ratios (8x and 16x) leads to a noticeable drop in SSIM, PSNR, and LPIPS performance. This demonstrates the limitations of static compression in preserving video fidelity. 2. **Dynamic VAE outperforms Static VAE:** The proposed DLFR-VAE framework consistently achieves higher reconstruction quality than its static counterpart across all resolutions, frame rates, and compression ratios. At a compression ratio of 6x, the performance of dynamic VAE is comparable to the Original VAE. At a compression ratio of 12x, the Dynamic VAE even surpasses the Static VAE at 8x in terms of reconstruction metrics, demonstrating the effectiveness of the adaptive approach in optimizing information retention. 3. **Generalizability of DLFR-VAE:** The performance gains of Dynamic VAE hold across different pretrained models,

Table 2. Video reconstruction performance on Open-Sora VAE. CR indicates the temporal compression ratio.

Size/FPS	VAE	CR	SSIM \uparrow	PSNR \uparrow	LPIPS \downarrow	rFVD \downarrow	FVMD \downarrow
540p/15	Original	4x	0.856	29.62	0.199	435	899
540p/15	Static	8x	0.746	27.31	0.245	1103	14311
540p/15	Static	16x	0.659	25.71	0.27	2164	15311
540p/15	Dynamic	6x	0.849	29.39	0.199	516	998
540p/15	Dynamic	8x	0.822	28.8	0.21	862	1085
540p/15	Dynamic	12x	0.762	27.44	0.229	1352	3577
540p/30	Original	4x	0.866	29.91	0.181	311	789
540p/30	Static	8x	0.781	27.99	0.229	986	13299
540p/30	Static	16x	0.702	26.23	0.257	1877	14311
540p/30	Dynamic	6x	0.864	29.9	0.177	340	823
540p/30	Dynamic	8x	0.849	29.3	0.188	499	1001
540p/30	Dynamic	12x	0.793	27.92	0.213	1277	3571
720p/15	Original	4x	0.884	30.73	0.179	305	799
720p/15	Static	8x	0.779	28.33	0.221	1003	13656
720p/15	Static	16x	0.692	26.6	0.244	2071	13699
720p/15	Dynamic	6x	0.877	30.42	0.182	551	863
720p/15	Dynamic	8x	0.85	29.78	0.192	737	1070
720p/15	Dynamic	12x	0.792	28.35	0.211	1232	2946
720p/30	Original	4x	0.897	31.22	0.159	320	534
720p/30	Static	8x	0.818	29.22	0.207	940	8848
720p/30	Static	16x	0.739	27.3	0.234	2131	8849
720p/30	Dynamic	6x	0.896	31.16	0.158	519	654
720p/30	Dynamic	8x	0.882	30.51	0.168	925	659
720p/30	Dynamic	12x	0.828	29.09	0.194	1345	1660

resolutions, and frame rates. This highlights the generality and robustness of the DLFR-VAE framework, making it suitable for a wide range of video generation tasks.

4.2. Visualization

To visually demonstrate the effectiveness of our DLFR-VAE framework, we present a comparison between the original video, the reconstruction result from the original HunyuanVideo VAE, and the reconstruction result from DLFR-HunyuanVideo VAE. As shown in Figure 5(a,b,c), our method dynamically adjusts the temporal compression ratio based on the complexity of the video content. Specifically, in scenes with rapid camera movements or high motion, DLFR-VAE employs a lower temporal compression ratio (i.e., a higher frame rate) to preserve temporal details. Conversely, in scenes with relatively static camera views or low motion, a higher compression ratio (i.e., a lower frame rate) is used to reduce computational overhead.

From a subjective visual perspective, the overall semantic content and motion coherence of the reconstructed video are well-preserved. However, there is a slight degradation in fine-grained details, particularly in regions with rapid local motion. For instance, at a compression ratio of 16x, some artifacts such as motion blur or ghosting may appear in areas with fast-moving objects.

It is important to note that DLFR-VAE is a training-free approach, meaning it does not require additional training or fine-tuning of the underlying VAE model. While this makes our method highly efficient and easy to integrate with existing systems [Kong et al., 2024; Zheng et al., 2024], the observed quality degradation in high-compression scenarios suggests potential areas for future improvement. For ex-

ample, fine-tuning the VAE or training it from scratch with dynamic frame rate adaptation could help mitigate these artifacts. Additionally, a more sophisticated approach could involve applying different frame rates to different regions of the video frame, addressing the trade-off between global and local motion preservation.

4.3. Ablation Study on Threshold

The threshold parameter, introduced in Equation 12, plays a critical role in determining the performance of the proposed DLFR-VAE. To better understand its impact, we conducted a grid search over different threshold values and evaluated the reconstruction performance. The results are visualized in Figure 6.

From Figure 6, the following observations can be drawn:

1. Across all tested threshold values, the performance of the **Dynamic VAE** consistently surpasses that of the **Static VAE**. This demonstrates the robustness and adaptability of the Dynamic VAE framework, as it effectively balances compression and reconstruction quality.
2. The presence of a well-defined Pareto curve [Blanchet et al., 2022] underscores the versatility of the Dynamic VAE across varying compression levels. This generalizability suggests that the model is capable of adapting to diverse use cases, from low-bitrate streaming to high-fidelity video reconstruction.

4.4. Video Generation in Dynamic Latent Space

In this section, we explore the feasibility of generating videos directly within a *Dynamic Frame Rate Latent Space* without any additional training. Given that contemporary image and video generation models are predominantly based on the Diffusion Transformer (DiT) architecture [Peebles & Xie, 2023; Esser et al., 2024], adapting these models to work in a dynamic latent space requires only minor adjustments.

To obtain the latent frame rates for different temporal segments of the generated video, we follow a multi-step process. First, we generate a preliminary video using a minimal number of denoising steps (e.g., 5 steps), which has a 10% computation cost of generating the video with 50 steps. Although this preliminary video has very low quality due to the limited number of steps, it still provides a clear indication of whether each video segment contains fast or slow motion. Based on this information, we then use the DLFR scheduler to assess the content complexity of each segment and determine the appropriate frame rate ratios. With these frame rate configurations, we proceed to generate the final videos in the dynamic frame rate latent space. To handle latent frames with varying frame rates, where a frame can represent either a short or long duration of time, we adjust the positional embedding for RoPE (Rotary Position Embedding) in DiT. Because tokens in the compressed latent space that each token represents a longer duration, we resample

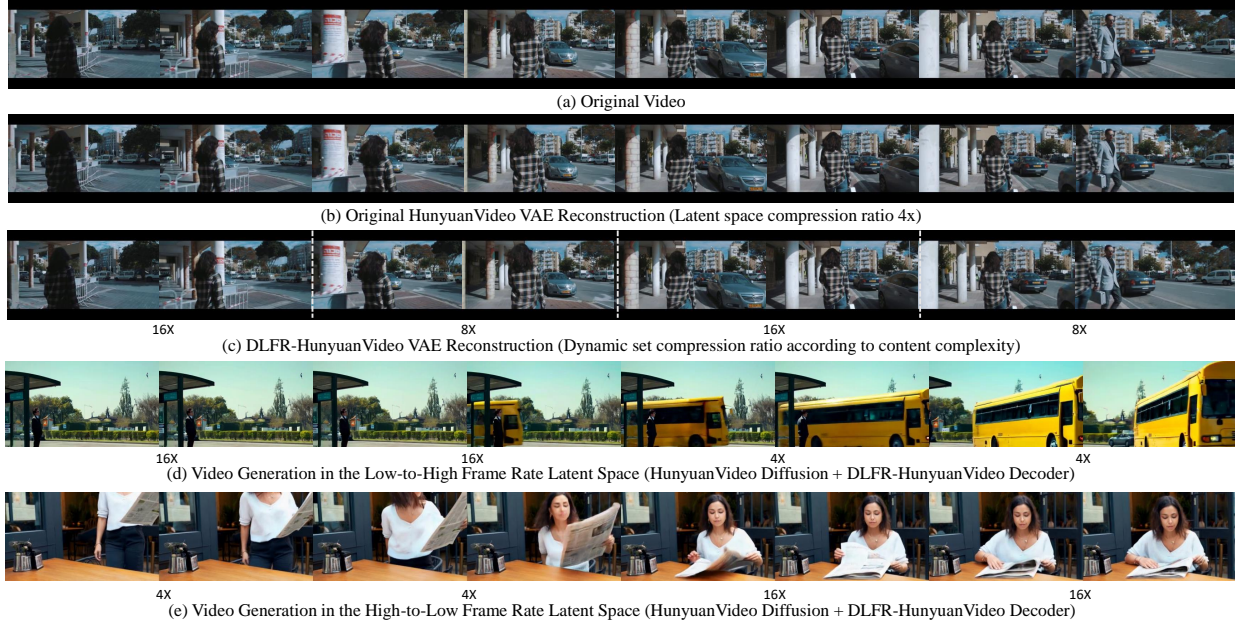


Figure 5. Comparison of the (a) original video, (b) the reconstruction result using the original HunyuanVideo VAE, and (c) the reconstruction result using our proposed DLFR-VAE. The figure illustrates the effectiveness of our dynamic frame rate adaptation in preserving video quality while reducing computational overhead. (d,e) The generated video in the dynamic latent space using the prompt: *Realistic style. A man stands at a quiet bus stop on a sunny afternoon. Then, a bright yellow bus approaches. and A woman strolls into a café and approaches a wooden table. She picks up a newspaper and starts reading it.*

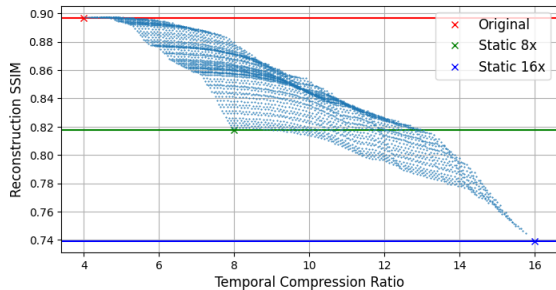


Figure 6. The influence of different threshold settings on OpenSora 720p 30fps videos. The threshold grid is made to cover the whole range of content complexity.

the cosine and sine parameters for RoPE². Finally, we apply our DLFR-VAE decoder to convert the latent representations into the final video output.

In Table 3, we present the results of generating videos at 480p resolution with 97 frames, based on a subset of prompts collected from VBench [Huang et al., 2024] with 21 prompts. To evaluate the alignment between text and video, we use CLIPSIM [Wu et al., 2021]. For assessing temporal consistency, we employ CLIP-Temp [Esser et al., 2023]. Additionally, we use VQA [Wu et al., 2022] to evaluate the aesthetic quality of the generated videos. We also measure temporal consistency, focusing on local and

²See Appendix for detail of the positional embedding parameter generation.

Table 3. Comparing the quality of video generation in raw latent space and our DLFR latent space. The end-to-end latency includes the preliminary video generation, dynamic frame rate schedule and the video generation in the compressed latent space.

	CLIP-T	CLIPSIM	VQA	FLICKER	Latency (s)
raw	0.9991	0.1869	97.56	0.9781	186
ours	0.9994	0.1874	97.44	0.9852	95

high-frequency details, using the temporal flickering score [Huang et al., 2024]. Our observations indicate that our approach achieves scores comparable to raw video generation while offering a 2x speedup.

In Figure 5(d,e), we show two videos with 1. High-to-Low Latent Frame Rate: Higher frame rates were applied to the initial temporal segments, followed by lower frame rates in subsequent segments. 2. Low-to-High Latent Frame Rate: Lower frame rates were applied to the earlier segments, gradually increasing to higher frame rates in later segments. Remarkably, even without retraining, the DiT-based neural network was able to produce coherent and visually plausible videos in the dynamic latent space.

5. Conclusion

In this paper, we introduced DLFR-VAE, a training-free framework for dynamic latent frame rate adaptation in video

generation. By dynamically adjusting the frame rate based on content complexity, DLFR-VAE significantly reduces the number of elements in latent space. Our experiments demonstrate its effectiveness across various resolutions and frame rates, showcasing its potential as a plug-and-play solution for existing video generation models.

Acknowledgment: We would like to express our gratitude to Xuefei Ning for her invaluable guidance and support throughout this research endeavor. We are also grateful to the NICS-efc Lab and Infinigence AI for their substantial support.

References

- Agarwal, N., Ali, A., Bala, M., Balaji, Y., Barker, E., Cai, T., Chattopadhyay, P., Chen, Y., Cui, Y., Ding, Y., et al. Cosmos world foundation model platform for physical ai. *arXiv preprint arXiv:2501.03575*, 2025.
- Ash, R. B. *Information theory*. Courier Corporation, 2012.
- Blanchet, T., Fournier, J., and Piketty, T. Generalized pareto curves: theory and applications. *Review of Income and Wealth*, 68(1):263–288, 2022.
- Brooks, T., Peebles, B., Holmes, C., DePue, W., Guo, Y., Jing, L., Schnurr, D., Taylor, J., Luhman, T., Luhman, E., Ng, C., Wang, R., and Ramesh, A. Video generation models as world simulators. 2024. URL <https://openai.com/research>.
- Chen, J., Cai, H., Chen, J., Xie, E., Yang, S., Tang, H., Li, M., Lu, Y., and Han, S. Deep compression autoencoder for efficient high-resolution diffusion models. *arXiv preprint arXiv:2410.10733*, 2024.
- Esser, P., Rombach, R., and Ommer, B. Taming transformers for high-resolution image synthesis. In *Proceedings of the IEEE/CVF conference on computer vision and pattern recognition*, pp. 12873–12883, 2021.
- Esser, P., Chiu, J., Atighehchian, P., Granskog, J., and Geramidis, A. Structure and content-guided video synthesis with diffusion models. In *Proceedings of the IEEE/CVF international conference on computer vision*, pp. 7346–7356, 2023.
- Esser, P., Kulal, S., Blattmann, A., Entezari, R., Müller, J., Saini, H., Levi, Y., Lorenz, D., Sauer, A., Boesel, F., et al. Scaling rectified flow transformers for high-resolution image synthesis. In *Forty-first International Conference on Machine Learning*, 2024.
- Fan, L., Li, T., Qin, S., Li, Y., Sun, C., Rubinstein, M., Sun, D., He, K., and Tian, Y. Fluid: Scaling autoregressive text-to-image generative models with continuous tokens. *arXiv preprint arXiv:2410.13863*, 2024.
- Feichtenhofer, C., Fan, H., Malik, J., and He, K. Slowfast networks for video recognition. In *Proceedings of the IEEE/CVF international conference on computer vision*, pp. 6202–6211, 2019.
- Ho, J., Jain, A., and Abbeel, P. Denoising diffusion probabilistic models. *Advances in neural information processing systems*, 33:6840–6851, 2020.
- Huang, Z., He, Y., Yu, J., Zhang, F., Si, C., Jiang, Y., Zhang, Y., Wu, T., Jin, Q., Chanpaisit, N., et al. Vbench: Comprehensive benchmark suite for video generative models. In *Proceedings of the IEEE/CVF Conference on Computer Vision and Pattern Recognition*, pp. 21807–21818, 2024.
- Jin, Y., Sun, Z., Li, N., Xu, K., Jiang, H., Zhuang, N., Huang, Q., Song, Y., Mu, Y., and Lin, Z. Pyramidal flow matching for efficient video generative modeling. *arXiv preprint arXiv:2410.05954*, 2024.
- Kingma, D. P. Auto-encoding variational bayes. *arXiv preprint arXiv:1312.6114*, 2013.
- Kondratyuk, D., Yu, L., Gu, X., Lezama, J., Huang, J., Schindler, G., Hornung, R., Birodkar, V., Yan, J., Chiu, M.-C., et al. Videopoet: A large language model for zero-shot video generation. *arXiv preprint arXiv:2312.14125*, 2023.
- Kong, W., Tian, Q., Zhang, Z., Min, R., Dai, Z., Zhou, J., Xiong, J., Li, X., Wu, B., Zhang, J., et al. Hunyuan-video: A systematic framework for large video generative models. *arXiv preprint arXiv:2412.03603*, 2024.
- Kuaishou. Kling video model. 2024. URL <https://kling.kuaishou.com>.
- Li, M., Lin, Y., Zhang, Z., Cai, T., Li, X., Guo, J., Xie, E., Meng, C., Zhu, J.-Y., and Han, S. Svdqnat: Absorbing outliers by low-rank components for 4-bit diffusion models. *arXiv preprint arXiv:2411.05007*, 2024a.
- Li, T., Tian, Y., Li, H., Deng, M., and He, K. Autoregressive image generation without vector quantization. *arXiv preprint arXiv:2406.11838*, 2024b.
- Li, X., Liu, C., Shuai, B., Zhu, Y., Chen, H., and Tighe, J. Nuta: Non-uniform temporal aggregation for action recognition. In *Proceedings of the IEEE/CVF Winter Conference on Applications of Computer Vision*, pp. 3683–3692, 2022.
- Li, X., Liu, Y., Lian, L., Yang, H., Dong, Z., Kang, D., Zhang, S., and Keutzer, K. Q-diffusion: Quantizing diffusion models. In *Proceedings of the IEEE/CVF International Conference on Computer Vision*, pp. 17535–17545, 2023.
- Lin, W., Chen, T., and Yu, C. Spvos: Efficient video object segmentation with triple sparse convolution. *IEEE Transactions on Image Processing*, 2023.
- Liu, J., Qu, Y., Yan, Q., Zeng, X., Wang, L., and Liao, R. Fr'echet video motion distance: A metric for evaluating motion consistency in videos. *arXiv preprint arXiv:2407.16124*, 2024.
- Lu, C., Zhou, Y., Bao, F., Chen, J., Li, C., and Zhu, J. Dpm-solver: A fast ode solver for diffusion probabilistic model sampling in around 10 steps. *Advances in Neural Information Processing Systems*, 35:5775–5787, 2022a.

- Lu, C., Zhou, Y., Bao, F., Chen, J., Li, C., and Zhu, J. Dpm-solver++: Fast solver for guided sampling of diffusion probabilistic models. *arXiv preprint arXiv:2211.01095*, 2022b.
- Ma, X., Fang, G., and Wang, X. Deepcache: Accelerating diffusion models for free. In *Proceedings of the IEEE/CVF Conference on Computer Vision and Pattern Recognition*, pp. 15762–15772, 2024a.
- Ma, Z., Zhang, Y., Jia, G., Zhao, L., Ma, Y., Ma, M., Liu, G., Zhang, K., Li, J., and Zhou, B. Efficient diffusion models: A comprehensive survey from principles to practices. *arXiv preprint arXiv:2410.11795*, 2024b.
- Mackin, A., Zhang, F., and Bull, D. R. A study of subjective video quality at various frame rates. In *2015 IEEE International Conference on Image Processing (ICIP)*, pp. 3407–3411. IEEE, 2015.
- Mackin, A., Zhang, F., and Bull, D. R. A study of high frame rate video formats. *IEEE Transactions on Multimedia*, 21(6):1499–1512, 2018.
- Menon, V. V., Feldmann, C., Amirpour, H., Ghanbari, M., and Timmerer, C. Vca: video complexity analyzer. In *Proceedings of the 13th ACM multimedia systems conference*, pp. 259–264, 2022.
- Nyquist, H. Certain topics in telegraph transmission theory. *Transactions of the American Institute of Electrical Engineers*, 47(2):617–644, 1928. doi: 10.1109/T-AIEE.1928.5055024.
- Papakonstantinou, T. Content based video encoding based on spatial and temporal information, 2023.
- Peebles, W. and Xie, S. Scalable diffusion models with transformers. In *Proceedings of the IEEE/CVF International Conference on Computer Vision*, pp. 4195–4205, 2023.
- Ravanbakhsh, E., Liang, Y., Ramanujam, J., and Li, X. Deep video representation learning: a survey. *Multimedia Tools and Applications*, 83(20):59195–59225, 2024.
- Rombach, R., Blattmann, A., Lorenz, D., Esser, P., and Ommer, B. High-resolution image synthesis with latent diffusion models. In *Proceedings of the IEEE/CVF conference on computer vision and pattern recognition*, pp. 10684–10695, 2022.
- Shang, Y., Yuan, Z., Xie, B., Wu, B., and Yan, Y. Post-training quantization on diffusion models. In *Proceedings of the IEEE/CVF conference on computer vision and pattern recognition*, pp. 1972–1981, 2023.
- Shannon, C. Communication in the presence of noise. *Proceedings of the IRE*, 37(1):10–21, 1949. doi: 10.1109/JRPROC.1949.232969.
- Song, H. and Kuo, C.-C. Rate control for low-bit-rate video via variable-encoding frame rates. *IEEE Transactions on Circuits and Systems for Video Technology*, 11(4): 512–521, 2001.
- Song, J., Meng, C., and Ermon, S. Denoising diffusion implicit models. *arXiv preprint arXiv:2010.02502*, 2020.
- Su, J., Ahmed, M., Lu, Y., Pan, S., Bo, W., and Liu, Y. Roformer: Enhanced transformer with rotary position embedding. *Neurocomputing*, 568:127063, 2024.
- Tian, K., Jiang, Y., Yuan, Z., Peng, B., and Wang, L. Visual autoregressive modeling: Scalable image generation via next-scale prediction. *arXiv preprint arXiv:2404.02905*, 2024.
- Vaswani, A. Attention is all you need. *Advances in Neural Information Processing Systems*, 2017.
- Wang, H., Shang, Y., Yuan, Z., Wu, J., Yan, J., and Yan, Y. Quest: Low-bit diffusion model quantization via efficient selective finetuning. *arXiv preprint arXiv:2402.03666*, 2024.
- Wu, C., Huang, L., Zhang, Q., Li, B., Ji, L., Yang, F., Sapiro, G., and Duan, N. Godiva: Generating open-domain videos from natural descriptions. *arXiv preprint arXiv:2104.14806*, 2021.
- Wu, H., Chen, C., Hou, J., Liao, L., Wang, A., Sun, W., Yan, Q., and Lin, W. Fast-vqa: Efficient end-to-end video quality assessment with fragment sampling. In *Proceedings of European Conference of Computer Vision (ECCV)*, 2022.
- Wu, J., Wang, H., Shang, Y., Shah, M., and Yan, Y. Ptq4dit: Post-training quantization for diffusion transformers. *arXiv preprint arXiv:2405.16005*, 2024a.
- Wu, P., Zhu, K., Liu, Y., Zhao, L., Zhai, W., Cao, Y., and Zha, Z.-J. Improved video vae for latent video diffusion model. *arXiv preprint arXiv:2411.06449*, 2024b.
- Xiang, X., Tian, Y., Zhang, Y., Fu, Y., Allebach, J. P., and Xu, C. Zooming slow-mo: Fast and accurate one-stage space-time video super-resolution. In *Proceedings of the IEEE/CVF conference on computer vision and pattern recognition*, pp. 3370–3379, 2020.
- Xing, Y., Fei, Y., He, Y., Chen, J., Xie, J., Chi, X., and Chen, Q. Large motion video autoencoding with cross-modal video vae. *arXiv preprint arXiv:2412.17805*, 2024.

- Yang, C., Xu, Y., Shi, J., Dai, B., and Zhou, B. Temporal pyramid network for action recognition. In *Proceedings of the IEEE/CVF conference on computer vision and pattern recognition*, pp. 591–600, 2020.
- Yu, S., Nie, W., Huang, D.-A., Li, B., Shin, J., and Anandkumar, A. Efficient video diffusion models via content-frame motion-latent decomposition. *arXiv preprint arXiv:2403.14148*, 2024.
- Yuan, Z., Zhang, H., Lu, P., Ning, X., Zhang, L., Zhao, T., Yan, S., Dai, G., and Wang, Y. Ditfastattn: Attention compression for diffusion transformer models. *arXiv preprint arXiv:2406.08552*, 2024.
- Zhang, Q. and Chen, Y. Fast sampling of diffusion models with exponential integrator. *arXiv preprint arXiv:2204.13902*, 2022.
- Zhang, R., Isola, P., Efros, A. A., Shechtman, E., and Wang, O. The unreasonable effectiveness of deep features as a perceptual metric. In *Proceedings of the IEEE conference on computer vision and pattern recognition*, pp. 586–595, 2018.
- Zheng, Z., Peng, X., Yang, T., Shen, C., Li, S., Liu, H., Zhou, Y., Li, T., and You, Y. Open-sora: Democratizing efficient video production for all. *arXiv preprint arXiv:2412.20404*, 2024.
- Zhu, Z., Feng, X., Chen, D., Bao, J., Wang, L., Chen, Y., Yuan, L., and Hua, G. Designing a better asymmetric vq-gan for stablediffusion. *arXiv preprint arXiv:2306.04632*, 2023.

A. Limitations and Future Directions

Although the current results are promising, there are also limitations. Firstly, although the generated videos using the compressed latent space exhibit good visual quality and high quality scores, they differ from those generated in the original latent space. Additionally, the lack of retraining prevents the generative model from fully exploiting the advantages of a dynamic latent space. Future research could address these limitations by: 1. Developing automated frame rate schedulers integrated with the generative process. 2. Designing new positional encoding mechanisms tailored to dynamic latent spaces. 3. Training generative models end-to-end in such spaces to maximize efficiency and performance.

B. Impact Statement

This paper presents work whose goal is to advance the field of Machine Learning, particularly in the domain of video generation. By introducing DLFR-VAE (Dynamic Latent Frame Rate Variational Auto Encoder), we propose a training-free framework that dynamically adjusts the latent frame rate based on video content complexity, significantly reducing computational overhead while maintaining high reconstruction quality. This innovation has the potential to make video generation more efficient and scalable, enabling longer and higher-resolution video synthesis with reduced computational resources.

The broader impact of this work includes potential applications in various fields such as entertainment, education, and virtual reality, where efficient video generation is crucial. By lowering the computational barriers, DLFR-VAE could democratize access to advanced video generation technologies, allowing smaller organizations and researchers with limited resources to leverage state-of-the-art video synthesis tools.

However, as with any generative technology, there are ethical considerations to be mindful of. The ability to generate high-quality videos efficiently could be misused for creating deepfakes or other forms of misinformation. It is important for the community to develop robust detection mechanisms and ethical guidelines to mitigate such risks. Additionally, the environmental impact of reduced computational requirements could be positive, as it may lead to lower energy consumption in data centers. While this work primarily aims to advance the technical capabilities of video generation, we encourage ongoing discussions around its ethical implications and societal consequences to ensure that the technology is used responsibly and for the benefit of society.

C. Design Details of Dynamic Upsampler / Down_sampler

We illustrate the design based on the 3D VAE with the 884 architecture adopted by HunyuanVideo. The encoder and decoder of this VAE consist of four down blocks / up blocks and a mid block, respectively.

In the encoder, temporal downsampling is achieved by the DownsampleCausal3D modules within certain down blocks, which apply convolutions with stride > 1 along the temporal dimension.

In the decoder, temporal upsampling is not performed via transposed convolution. Instead, each up block restores the temporal sequence length using interpolation (e.g., nearest-neighbor), followed by convolutions with stride $= 1$ for feature fusion and smoothing.

DLFR operates **only** along the temporal dimension. The design and positional selection of the upsampler/down_sampler are as follows:

Temporal Downsampling in the Encoder: We modify the temporal stride of the DownsampleCausal3D modules in selected down blocks — for example, changing the stride from $(1, 2, 2)$ to $(2, 2, 2)$, or from $(2, 2, 2)$ to $(4, 2, 2)$ — where (T, H, W) denotes temporal, height, and width dimensions, respectively. This enables a further increase in the temporal downsampling ratio.

Temporal Downsampling Positional Selection: Among the four down blocks, only the first three (closer to the input) contain DownsampleCausal3D modules, thus offering three selectable positions. For $2\times$ **downsampling**, one of the three down blocks is selected and its stride is modified; for $4\times$ **downsampling**, two of them are selected for stride adjustment.

Temporal Upsampling in the Decoder: Each up block contains three ResNet blocks and one interpolation module. To perform upsampling, we insert an additional nearest-neighbor interpolation module either *before* or *after* a selected ResNet block to increase the temporal resolution.

Temporal Upsampling Positional Selection: Across the four up blocks, there are 12 ResNet blocks. Considering both pre- and post-insertion for each, we obtain 16 candidate positions. For $2\times$ **upsampling**: one interpolation location is selected; for $4\times$ **upsampling**: two positions are selected.

Optimal Combination Selection: To determine the best combinations of upsampling and downsampling positions, we exhaustively evaluate all possible configurations by constructing corresponding VAE models. For **2 Hz** frame rate: there are 48 possible combinations; for **4 Hz** frame rate: there are 546 possible combinations. These are tested on 500

videos at 15 Hz and 540p resolution. Evaluation metrics include **SSIM**, **PSNR**, and **LPIPS**.

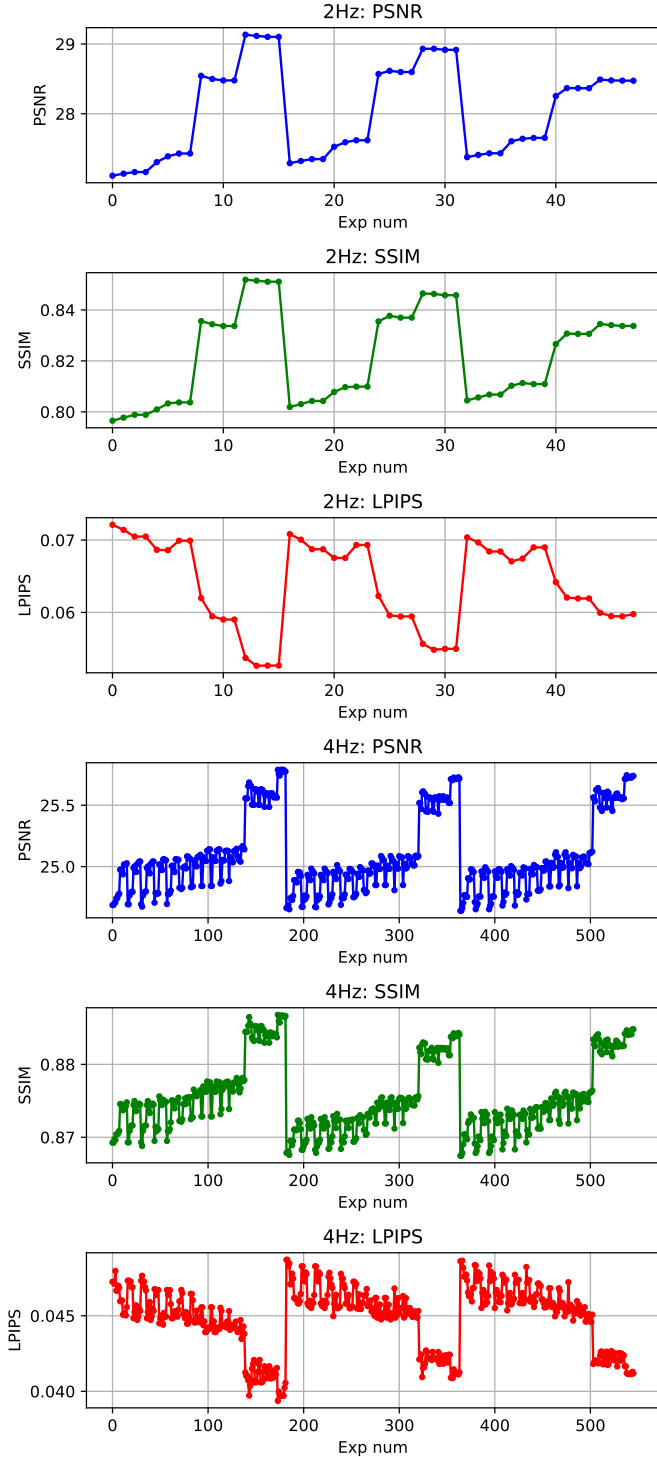


Figure 7. VAE reconstruction metrics (SSIM, PSNR, LPIPS) under different frame rates and combinations.

Results: The results (see Figure 7) indicate that the three evaluation metrics (SSIM, PSNR, LPIPS) follow a highly consistent pattern across all configuration combinations. Specifically, configurations achieving the highest SSIM and PSNR values also tend to yield the lowest LPIPS scores. Notably, the most effective upsampling and downsampling positions are predominantly located near the input end of the encoder and the output end of the decoder.

Based on this analysis, we fix the optimal position combinations under each frame rate setting for use in subsequent experiments and system deployment.

D. Video Generation with Modified RoPE

For video generation on the dynamic frame rate latent space, we modify the RoPE in of the diffusion transformer (DiT). To handle latent frames with varying frame rates, where a frame can represent either a short or long duration of time, we adjust the positional embedding for RoPE (Rotary Position Embedding) in DiT. Specifically, for tokens in the compressed latent space that each token represents a longer duration, we reduce the frequency of the RoPE parameters to generate the cosine and sine components.

D.1. Concept of RoPE

The RoPE (Rotary Position Embedding) mechanism is a technique used in transformer-based models [Su et al., 2024], including those applied in diffusion models like Diffusion Transformer. We first provides a detailed introduction to the RoPE mechanism in the context of Diffusion Transformer.

In transformer models, position embeddings are crucial for the model to understand the order of input elements (e.g., tokens in a sequence). Traditional position embeddings (like those in the original Transformer model) use fixed vectors to represent positions, which can be inefficient for long sequences and may not generalize well to sequences of different lengths. RoPE addresses these limitations by introducing a more dynamic way of encoding positions.

RoPE represents positions using a combination of sine and cosine functions. For a token at position m with embedding $\mathbf{x}_m \in \mathbb{R}^D$, RoPE applies rotation matrices \mathbf{R}_m to queries (\mathbf{q}_m) and keys (\mathbf{k}_n) in the attention mechanism:

$$\mathbf{q}_m = \mathbf{R}_m \mathbf{W}_q \mathbf{x}_m, \quad \mathbf{k}_n = \mathbf{R}_n \mathbf{W}_k \mathbf{x}_n \quad (16)$$

where \mathbf{R}_m is defined block-diagonally for each dimension pair $(2i, 2i + 1)$:

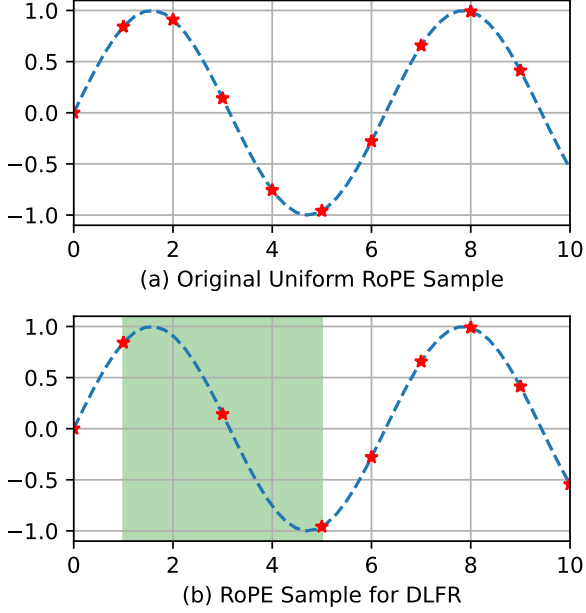


Figure 8. Illustration of resampling for DLFR. (a) represents the original RoPE sampling method, while (b) depicts the resampling method adapted for DLFR. The green areas highlight the extended positional relationships for tokens that represent longer time spans.

$$\mathbf{R}_m = \bigoplus_{i=1}^{D/2} \begin{pmatrix} \cos m\theta_i & -\sin m\theta_i \\ \sin m\theta_i & \cos m\theta_i \end{pmatrix}, \quad \theta_i = 10000^{-2i/D} \quad (17)$$

The attention score $A_{m,n}$ naturally encodes relative positions:

$$A_{m,n} = (\mathbf{R}_m \mathbf{q}_m)^\top (\mathbf{R}_n \mathbf{k}_n) \quad (18)$$

The frequency of the RoPE is $10000^{-2i/D}$.

D.2. Resample RoPE Parameters for DLFR

When a latent token corresponds to a longer time span, the RoPE parameters should be adjusted. This is because such tokens encode positional relationships over longer temporal intervals compared to adjacent frames.

To address this, we replace the m in Equation 18 with P_m based on the frame rates of different tokens. For a token with longer time span, its positional distance to neighboring tokens increases proportionally. Using this relationship, we compute the new RoPE parameters as follows:

In this way, we generate the new RoPE parameters:

Table 4. Latency of one diffusion step under different latent space on HunyuanVideo Diffusion model.

		Original	DLFR	DLFR	DLFR	
		CR	4x	6x	8x	12x
720p	latency	59.90	29.36	19.26	9.58	
	speedup	1.00	2.04	3.11	6.25	
540p	latency	24.93	11.61	7.73	4.05	
	speedup	1.00	2.15	3.23	6.16	

$$\mathbf{R}_m = \bigoplus_{i=1}^{D/2} \begin{pmatrix} \cos P_m \theta_i & -\sin P_m \theta_i \\ \sin P_m \theta_i & \cos P_m \theta_i \end{pmatrix}, \quad \theta_i = 10000^{-2i/D} \quad (19)$$

As shown in Figure 8, the interval of different RoPE sample points is different according to the frame rate.

D.3. Speedup of generating videos in compressed space

We evaluated the latency of denoising step of different compression ratio. From Table 4, we observe that denoising in the compressed latent space can significantly reduce the generation cost. At CR=6x, it achieves an average speedup of 2x for one step of denoising. At CR=12x, DLFR achieves a speedup of more than 6x. These improvements primarily stem from the reduction in the number of tokens processed by the diffusion model. Since the computational complexity of the Transformer’s attention mechanism scales quadratically with the number of tokens, reducing the token count leads to substantial computational savings.